14th World Congress on Computational Mechanics (WCCM)
ECCOMAS Congress 2020)
Virtual Congress: 11-–15 January 2021
F. Chinesta, R. Abgrall, O. Allix and M. Kaliske (Eds)

A $P1/P1$ FINITE ELEMENT FRAMEWORK FOR TAKING INTO ACCOUNT CAPILLARY EFFECTS IN BIPHASIC FLOW SIMULATIONS

L. CHEVALIER[1], J. BRUCHON[1], N. MOULIN[1], P.-J. LIOTIER[2] AND DRAPIER[1]

[1] Mines Saint-Étienne, Univ Lyon, CNRS, UMR 5307 LGF, Centre SMS
F - 42023 Saint-Étienne, France
{bruchon,nmoulin,drapier}@emse.fr

[2] Centre des Matériaux des Mines d'Alès (C2MA), IMT Mines Alès, Université de Montpellier
30319 Alès CEDEX, France
pierre-jacques.liotier@mines-ales.fr

Key words: triple junction, permeability, capillary pressure, fibrous media

Abstract. This work describes a computational strategy, based on a stabilised finite element method, to simulate bifluid flow with capillary effects in a fibrous microstructure. In this framework, triple junction equilibrium is imposed as a natural condition in the weak formulation of the Stokes problem. Two types of 2D microstructures are then considered, hexagonal and random, and studied in terms of numerical permeability and capillary pressure.

1 Introduction

Capillarity can be defined as the ability of a liquid to maintain contact with a solid substrate without the need for external forces. Capillary effects, which occur when three phases (liquid, gas and solid) are in presence, are involved in many areas of engineering. For example, their influence has been demonstrated during the resin infusion manufacturing process of composite materials [1]. In the context of the simulation of such manufacturing processes, this work aims at proposing a finite element strategy to simulate capillary flows at the fibre scale. The rest of this paper is organized as follows. The mathematical model developed is presented in Section 2: Stokes equations and associated interface or boundary conditions. The weak formulation of this problem is given is Section 3, as well as the computational strategy employed. Finally, two type of microstructures (hexagonal and random) are investigated in Section 4. Quantities of interest, such as capillary pressure, are computed from these digital microstructures and compared to measured or reference values.

2 Mathematical model

Let Ω be the computational domain, a bounded region of $\mathbb{R}^d$, with $d = 2,3$ the space dimension. This domain describes the fibrous microstructure through which a Newtonian fluid flows. Fibres are assumed to be rigid and therefore represented by holes into Ω. This configuration is sketched in Figure 1. The computational domain also contains a "surrounding medium", *i.e.* a gas phase. Consequently: $\Omega = \Omega_l \cup \Omega_g$, where Ω_l and Ω_g are the liquid and gas subdomains respectively. The liquid - gas interface is

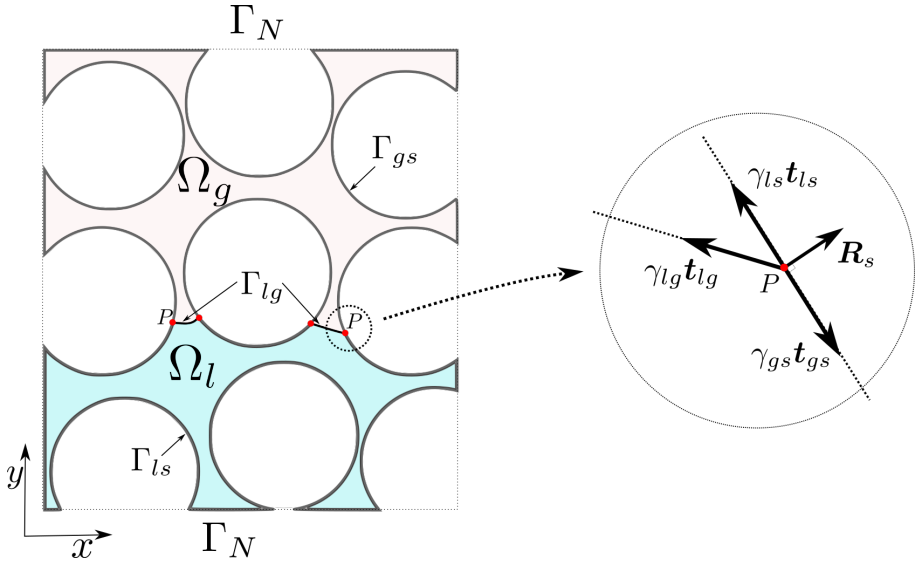

Figure 1: Computational domain Ω and zoom-in on a triple point

denoted Γ_{lg}, while Γ_{ls} and Γ_{gs} denote the liquid - solid and gas - solid interfaces. Finally, the intersections between these three interfaces define the triple junctions. They are points in 2D situations like those investigated in this paper (points P in Figure 1) and lines in 3D cases like those treated in [2].

2.1 Mechanical equilibrium in bulk

Both liquid and gas as considered as incompressible Newtonian fluids, characterized by their viscosities, respectively η_l and η_g, with $\eta_g \ll \eta_l$, and their densities ρ_l and ρ_g. Note that our purpose is not to obtain a fine description of gas dynamics, but just, in an Eulerian framework, to extend the velocity and pressure fields to the whole computational domain, without disturbing the liquid flow. Since the inertia effect is neglected in this paper, momentum and mass balances give rise to the usual Stokes system

$$-\nabla\cdot(2\eta\dot{\varepsilon}(v))+\nabla p = \rho g \quad \text{in } \Omega \tag{1}$$

$$\nabla\cdot v = 0 \quad \text{in } \Omega \tag{2}$$

with $\dot{\varepsilon}(v)=(\nabla v+\nabla^T v)/2$ the strain rate tensor, g the gravitational acceleration, η equal to η_l in Ω_l and η_g in Ω_g, and ρ equal to ρ_l in Ω_l and ρ_g in Ω_g.

These equations are closed by considering the interface and boundary conditions given in the following that characterize capillary flows.

2.2 Mechanical equilibrium at interfaces

Liquid - gas interface. The action exerted by the liquid and gas domains on the interface Γ_{lg} is described by the stress vectors $-\sigma_l\cdot n$ and $\sigma_g\cdot n$, where $\sigma_{l/g}=2\eta_{l/g}\dot{\varepsilon}(v)-pI$ is the liquid/gas Cauchy stress tensor, and n the unit normal to the interface, pointing outward the liquid part. In addition, let us consider a surface stress, distributed over Γ_{lg}, and given by a vector field T. Due to the angular momentum balance, T must be tangential to the interface: $T=\gamma_{lg}t_{lg}$, where the scalar γ_{lg} is the surface tension parameter

and t_{lg} the unit tangent to the interface, defined as the derivative of the position vector with respect to arclength s. Finally, the force balance on the interface writes [2, 3]:

$$[\sigma \cdot n]_{\Gamma_{lg}} = -\frac{d}{ds}(\gamma_{lg} t_{lg}) \tag{3}$$

where $[\sigma \cdot n]_{\Gamma_{lg}}$ is the stress vector jump across Γ_{lg}.

Note that, expanding the derivative in the right-hand-side and using the Frenet-Serret formula $dt_{lg}/ds = \kappa n$ (κ is the mean curvature), provides two terms: one is the usual curvature term of Laplace's law, related to the jump in normal stress; the other is the surface derivative of γ_{lg}, related to the jump in shear stress (Magangoni's effect).

Fluid - solid interfaces. The solid substrate, assumed to be a rigid body, is represented by a boundary of the computational domain. The above observations allow us to write, with coherent notations:

$$\sigma_l \cdot n = \frac{d}{ds}(\gamma_{ls} t_{ls}) \text{ on } \Gamma_{ls} \text{ and } \sigma_g \cdot n = \frac{d}{ds}(\gamma_{gs} t_{gs}) \text{ on } \Gamma_{gs} \tag{4}$$

Note that, a Navier friction law, not presented here, can also be considered in (4) [2].

2.3 Mechanical equilibrium at triple junctions

Triple junctions are the locus defined by the intersections of Γ_{lg}, Γ_{ls} and Γ_{gs}. For example, they are the set of points P represented in Figure 1 in a 2D context. In these points, the mechanical equilibrium writes:

$$\gamma_{lg} t_{lg} + \gamma_{ls} t_{ls} + \gamma_{gs} t_{gs} = -R_s \tag{5}$$

where R_s is the substrate reaction, here perpendicular to its surface due to the rigid body assumption. Therefore, this vector has no influence on the flow.

2.4 Boundary conditions

Previous interface conditions are completed as it follows. Let Γ_N be the lower and upper boundaries of the computational domain (see Figure 1). Then:

$$\sigma \cdot n = -p_{ext} n \text{ on } \Gamma_N \tag{6}$$

where p_{ext} is an external pressure. Additionally, considering $\Gamma_D = \partial\Omega \backslash \Gamma_N$, we have

$$v \cdot n = 0 \text{ on } \Gamma_D, \tag{7}$$

and

$$(\sigma \cdot n) \cdot t = 0 \text{ on } \Gamma_D \backslash (\Gamma_{ls} \cup \Gamma_{gs}) \tag{8}$$

Finally, the capillary flow of a liquid in a microstructure, is described by the Stokes equations (1)-(2) completed with conditions (3)-(8).

3 Numerical strategy

Flow equations in the previous section are solved using a finite element method combined with a level-set technique to capture the evolution of the liquid - gas interface. Before detailing these points, let us introduce the weak formulation of the capillary flow problem.

3.1 Weak formulation

The key point of the approach presented here is to treat interface conditions (3)-(4) and equilibrium at triple junctions (5) as Neumann conditions which are consequently weakly imposed. The weak form of the problem is a direct result of the following relations. Let $w : \Omega \to \mathbb{R}^d$ be a velocity test function with the property that $w \cdot n = 0$ on Γ_D. By summing the contributions of Ω_l and Ω_g, we have:

$$\begin{aligned} -\int_\Omega w \cdot \nabla \cdot \sigma \, dv &= \int_\Omega \sigma : \nabla w \, dv + \int_{\Gamma_N} p_{ext} w \cdot n ds \\ &\quad - \int_{\Gamma_{lg}} w \cdot \frac{d}{ds}(\gamma_{lg} t_{lg}) \, ds - \int_{\Gamma_{ls}} w \cdot \frac{d}{ds}(\gamma_{ls} t_{ls}) \, ds - \int_{\Gamma_{gs}} w \cdot \frac{d}{ds}(\gamma_{gs} t_{gs}) \, ds \end{aligned} \tag{9}$$

Next, integrating by part on each interface Γ_i, with $i \in \{lg, ls, gs\}$:

$$\int_{\Gamma_i} w \cdot \frac{d}{ds}(\gamma_i t_i) \, ds = -\int_{\Gamma_i} \gamma_i t_i \cdot \frac{dw}{ds} + \int_{\partial\Gamma_i} \gamma_i w \cdot t_i \varsigma ds \tag{10}$$

Here, several remarks can be done. First, $t \cdot \frac{dw}{ds}$ is nothing but the surface divergence of w, which can be rewritten in tensor notation [2] as: $(I - n \otimes n) : \nabla w$. Second, in a 2D case, the boundary $\partial\Gamma_i$ of the curve Γ_i is reduced to two points, the two extremities of the curve. Hence, in such a situation, the last integral of Equation (10) is nothing more than the sum of the values of $\gamma w \cdot t \varsigma$ taken at these points. In addition, ς is equal to $+1$ or -1 at each extremity of Γ_i, depending on the chosen orientation (in 3D, ς is a unit vector, tangent to the surface and normal to the curve). It is important to note that when one extremity of Γ_i is a triple point, Equation (9) shows that equilibrium condition (5) can be weakly imposed at this point. The term $w \cdot R$ which results from the sum of the different contributions, is equal to zero. Indeed, on the one hand, the reaction of the substrate, R, is collinear with n, the normal to the solid surface, on the other hand $w \cdot n = 0$. Finally, in the case where one extremity of Γ_i is not a triple point, we will assume, for simplicity, that the associated boundary term $w \cdot t_i$ vanishes. If not, this term must be taken into account in the weak formulation.

In the end, the weak form of the Stokes problem, including capillary effects, writes: find $(v, p) \in H^1(\Omega)^d \times L^2(\Omega)$, $v \cdot n = 0$ on Γ_D, such as

$$\begin{aligned} &\int_\Omega \eta \nabla v : \nabla w \, dv - \int_\Omega p \nabla \cdot w \, dv = \\ &\qquad \int_\Omega \rho g \cdot w \, dv - \int_{\Gamma_N} p_{ext} w \cdot n \, ds - \int_{\Gamma_{lg} \cup \Gamma_{ls} \cup \Gamma_{gs}} \gamma (I - n \otimes n) : \nabla w \, ds \\ &\int_\Omega q \nabla \cdot v \, dv = 0 \end{aligned} \tag{11}$$

for all couple of test functions $(w, q) \in H^1(\Omega)^d \times L^2(\Omega)$, with $w \cdot n = 0$ on Γ_D. Moreover, γ is equal to γ_{lg}, γ_{ls}, γ_{gs} on the corresponding interfaces.

3.2 Finite element approximation

The computational domain is discretised using an unstructured mesh, made up of triangles in 2D or tetrahedrons in 3D. In a Finite Element (FE) framework, both velocity and pressure are approximated by piecewise linear continuous discrete fields v_h and p_h. Such a $P1/P1$ mixed FE does not lead to a well-posed formulation of the discrete Stokes problem. This difficulty is overcome by the use of a Variational MultiScale (VMS) stabilisation technique, consisting in splitting the unknowns in a computable component, the FE solution, and an uncomputable one that cannot be captured by the FE mesh: $v = v_h + \tilde{v}$ and $p = p_h + \tilde{p}$. More specifically, the *Algebraic SubGrid Scale* (ASGS) method is employed in this work. Developed by Badia and Codina [4], this approach consists in approximating the subgrid terms $\tilde{v}$ and $\tilde{p}$ by quantities proportional to the residuals of the Stokes equations, and results in stabilization terms consistently added to the FE formulation.

Due to the liquid - gas interface curvature, pressure is intrinsically discontinuous across this interface. However, the discretisation given so far implies a continuous discrete pressure field, which therefore cannot accurately capture the discontinuity and leads to oscillations. That is why, in the elements crossed by the interface, the pressure approximation space is enriched by two discontinuous shape functions. This strategy, proposed by Ausas *et al.* in [5], does not increase the size of the final linear system, since the degrees of freedom associated with the enrichment can be condensed prior to the assembling of the global matrix. In addition, a similar strategy due to Coppola-Owen and Codina [10] can be employed to capture the discontinuity in the pressure gradient that results in the jump of viscosity across the liquid - gas interface.

3.3 Semi-implicit discretisation of the surface tension term

The discretisation of the Stokes problem leads to spurious velocity oscillations, also called parasitic currents, located in the vicinity of the liquid - gas interface. In the work discussed here, these perturbations are due, on the one hand, to the pressure approximation, even though the enrichment technique greatly improves the situation, and on the other hand, to the piecewise linear approximation of the interface which can give rise to artificial curvatures. These non-physical velocities cause small oscillations of the interface: this is the phenomenon of capillary wave propagation, with a wavelength of the same order as the mesh size. Denner and van Wachem have shown in [6] that whatever the time coupling between the resolution of the mechanical problem and the transport of the interface, these discretisation errors will increase over time if the time step does not satisfy some restrictions. However, in practical situations, these restrictions make the time step too small to carry out simulations. In the literature, this limitation is typically overcome by considering a semi-implicit form of the surface tension term $\int_{\Gamma_{lg}} \gamma_{lg}(I - n \otimes n) : \nabla w \, ds$. This integral is then evaluated by using a prediction of the position of the interface at the next time increment, which gives the following additional term in the problem formulation:

$$\Delta t \int_{\Gamma_{lg}} \gamma_{lg}(\nabla v \cdot (I - n \otimes n)) : \nabla w \, ds \tag{12}$$

where Δt is the time step. This interface shear stress dissipates surface energy, especially at small wavelength, thus avoiding capillary wave propagation.

3.4 Interface transport

The interface Γ_{lg} is implicitly described as the zero-isovalue of a level-set function ϕ_h, continuous over the computational domain, piecewise linear, positive in the gas subdomain and negative in the liquid subdomain. Initially, ϕ_h is chosen as the signed distance to the interface, filtered by a hyperbolic tangent [2, 3]. At each instant t_n, the velocity $v_h(t_n)$ and the pressure $p_h(t_n)$ are computed on the configuration corresponding to $\phi_h(t_n)$. $\phi_h(t_{n+1})$ is subsequently computed by solving the transport equation

$$\frac{\partial \phi_h}{\partial t}(t_{n+1}) + v_h(t_n) \cdot \nabla \phi_h(t_{n+1}) = 0 \tag{13}$$

using a SUPG stabilisation technique. Note that this weak coupling between mechanics and geometry can be improved by solving iteratively in the same time increment, both the Stokes and transport equations, until reaching a global convergence on $(v_h, p_h, \phi_h)(t_{n+1})$. This strong coupling allows a better accuracy on the contact angle between liquid and solid [8]. However, this strategy also has a higher computation cost. Here, only the weak coupling is used.

Finally, we mention that the surface integrals in Equation (11) are computed by local reconstruction of the interface as a segment (or a 3D plane) in the elements cut by the interface. In addition, the volume quadrature rule is enriched in these elements in order to take into account viscosity and density discontinuities.

4 Simulation results

The computational strategy presented above has been implemented in the FE *Z-set* software. The relevance of this approach has been evaluated in references [3, 2, 8] with 2D and 3D simulations of droplet spreading and capillary rise. Among other results, the contact angle provided by the simulations is equal to that of the Young - Laplace equation, as expected, at least as long as no dissipation is considered at the triple junction (see [2]). This work presents simulations of capillary rise into two different microstructures, and sketches first calculations of capillary pressure. The two structures are: a hexagonal arrangement of circular (half-)fibers disposed in staggered rows (structure 1) with a fiber volume ratio V_f of 52%; a random microstructure (structure 2) made up of identical circular fibers with $V_f = 48\%$ [9]. In both cases, the fiber radius is of $5\,\mu$m. The surface tension and energies are $\gamma_{lg} = 37.03 \times 10^{-3}$ N/m, $\gamma_{ls} = 30.03 \times 10^{-3}$ N/m and $\gamma_{gs} = 60.93 \times 10^{-3}$ N/m. The liquid viscosity is $\eta_l = 10^{-3}$ Pa.s, that of the surrounding medium is $\eta_g = 1.71 \times 10^{-5}$ Pa.s, and the gravity is neglected. Figures 2a and 2b show at a given time, the liquid - gas interface (green line), the velocity and pressure isovalues, as well as the streamlines, during a capillary rise in structures 1 and 2.

4.1 Expression of the capillary pressure

The calculation of an "equivalent" capillary pressure p_{cap} proposed here, is carried out by considering a unidirectional flow in a homogeneous medium equivalent to structures 1 or 2. The flow in this medium is described by Darcy law

$$v_d = -\frac{K}{\eta} \nabla p_d \tag{14}$$

where K is the permeability of the porous medium, here assumed isotropic, v_d and p_d are the Darcy velocity and pressure, formally defined as the Stokes velocity and pressure averaged on an elementary

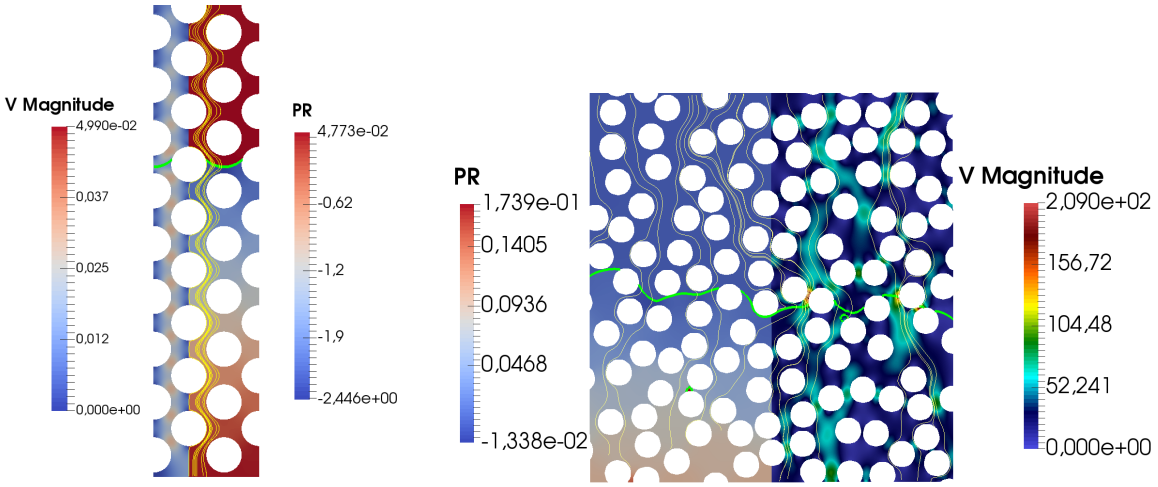

(a) Structure 1 (b) Structure 2

Figure 2: Capillary rise in hexagonal (structure 1) and random (structure 2) structures: flow front, pressure, velocity intensity and streamlines.

volume of the microstructure. In this context, the action of capillary forces is expressed as a pressure discontinuity across the liquid - gas interface, resulting in a pressure jump equal to p_{cap}. Under such conditions, it can be demonstrated analytically (see reference [1]), that the liquid height $h(t)$ is given, assuming $h(t=0)=0$, by

$$h(t) = \frac{1}{\eta_l - \eta_g}\left(\sqrt{2(\eta_l-\eta_g)K(p_{cap}-\Delta p)t + h_{max}^2\eta_g^2} - h_{max}\eta_g\right) \tag{15}$$

where Δp is the difference of pressure imposed as a boundary condition between the inlet (up) and outlet (down) sides; h_{max} is the maximum height that the liquid can reach, typically the size of the computational domain. Neglecting the gas viscosity, *i.e.* $\eta_g \ll \eta_l$, the expression of capillary pressure we propose is

$$p_{cap}(t) = \frac{\eta_l h^2(t)}{2Kt} + \Delta p \tag{16}$$

Note that if h^2 has a linear dependence in time, as in 1D Darcy law, p_{cap} would be independent of time. In the following, this relation is used to define p_{cap} for Stokes flows in structures 1 and 2. However, before dealing this point, the permeability of these structures must be determined.

4.2 Permeability calculation

Permeability is computed for saturated flows. Consequently, capillary phenomena play no role in this computation. Two approaches can be used.

- The first approach is based on the Darcy law formulated in term of flow rate Q,

$$Q = -\frac{K}{\eta_l}|S|\frac{\Delta p_K}{h_{max}} \tag{17}$$

where, Δp_K is the total pressure drop imposed at boundaries, which forces the fluid to flow, h_{max} is the height of the Stokes domain, and $|S|$ is the area of the S cross-section through which Q the flux computed. Hence, we also have $Q = \int_S v \cdot n ds$. Once the Stokes equations have been solved, permeability K can be calculated by identifying these two expressions.

- The second approach considers the Darcy velocity and pressure as averaged quantities obtained from the Stokes fields by homogenization over an elementary volume [7]:

$$v_d = \frac{1}{|\Omega|} \int_{\Omega_l} v dv \quad \text{et} \quad p_d = \frac{1}{|\Omega_l|} \int_{\Omega_l} p dv \tag{18}$$

As with the first approach, once the Stokes equations have been solved, the values of v_d and p_d can be post-processed and injected in the Darcy law (14) to obtain the permeability.

The permeability corresponding to the hexagonal packing is found to be $K = 2.25 \times 10^{-13}$ m^2 with the first approach, and $K = 5.5 \times 10^{-13}$ m^2 with the second. These values are obtained with a computational domain that has become representative in the sense that the permeability does not change as the size of the domain increases. Such a representative domain contains 40 fibres. Note also that these values are of the same order as those provided by the Gebart model [11], $K_G = 3,4 \times 10^{-13}$ m^2 for a hexagonal configuration and a Stokes flow. The permeability given by the Kozeny-Carman model [12] is also very close: $K_{KC} = 2.3 \times 10^{-13}$ m^2 , for a $V_f = 52\%$ and a fibre radius equal to 5μ m. For the random structure with $V_f = 48\%$, several elementary volume sizes are considered, ranging from 200 to 1000 fibres. For each size, 15 samples of the structure are generated. It is shown that the convergence on permeability is achieved with 600 fibres: the mean value is then $K = 5 \times 10^{-13}$ m^2 with Method 1, $K = 1.4 \times 10^{-12}$ m^2 with Method 2, and the corresponding standard deviations are respectively 3×10^{-14} m^2 and 4×10^{-14} m^2 respectively. Note that, as mentioned in [8], Method 2 provides an upper bound of permeability.

4.3 Results and discussion

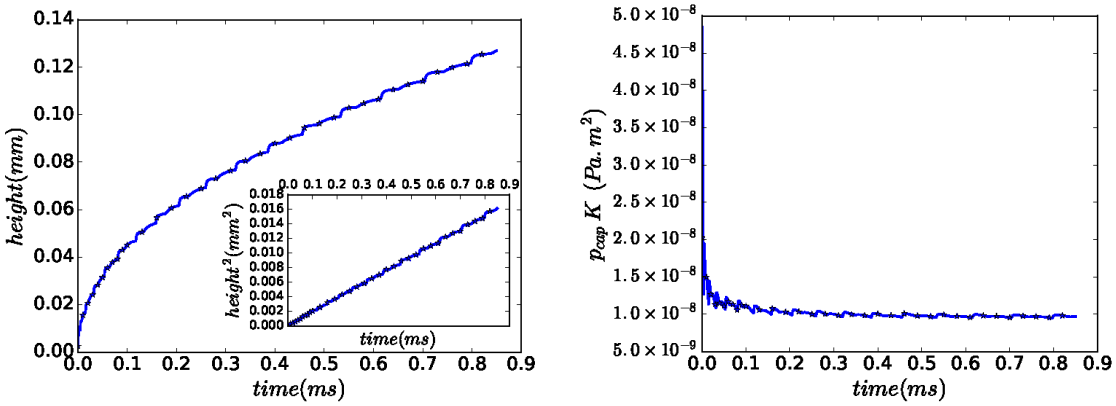

(a) $h(t)$ and $h^2(t)$ (b) $\eta_l h^2(t)/2t = p_{cap} \times K$

Figure 3: Capillary rise in a hexagonal structure: average position of the flow front over time (a) and corresponding values of $p_{cap}K$ (b).

The capillary rise into a hexagonal structure is first investigated, with a pressure drop equal to zero:

$p_{ext} = 0$, $\Delta p = 0$. The average liquid height $h(t)$ is plotted over time in Figure 3a, while Figure 3b shows the quantity $\frac{\eta_l h^2(t)}{2t}$, which corresponds, according to Equation (16), to $p_{cap}K$, the product between capillary pressure and permeability. Except for the very first time increments of the simulation (Equation (16) is not valid at $t = 0$), $p_{cap}K$ fluctuates around a steady value of 1.0×10^{-8} Pa.m^2, leading to a capillary pressure $p_{cap} \approx 0.44$ bar or $p_{cap} \approx 0.18$ bar, depending on the Method (1 or 2) considered for calculating the permeability. These values are consistent with those determined experimentally [1]. These results also mean that, in the case of a Stokes flow whose driving force is capillarity alone, the average position of the flow front, $h(t)$, behaves as the square-root of time, or, equivalently, that its velocity decreases as $1/h(t)$. The subfigure in Figure 3a clearly shows that the quantity $h^2(t)$ is linear in time.

Next, the capillary rise into a random structure with $V_f = 48\%$ (Figure 2b) is examined. A spontaneous capillary rise of the resin cannot be fully achieved in this case: the gap between two neighbouring fibres can be large enough to allow a stationary state of the flow front, *i.e.* a state of zero-curvature satisfying the equilibrium at the triple points (5). Note that the contacts between fibres should be much higher in a real 3D fibrous microstructure, thus facilitating capillarity. Here, an additional driving force, *i.e.* a pressure drop, forces the liquid to flow: $p_{ext} = 2$ kPa is set on the inlet boundary, $p_{ext} = 0$ on the outlet boundary, resulting in $\Delta p = -2$ kPa.

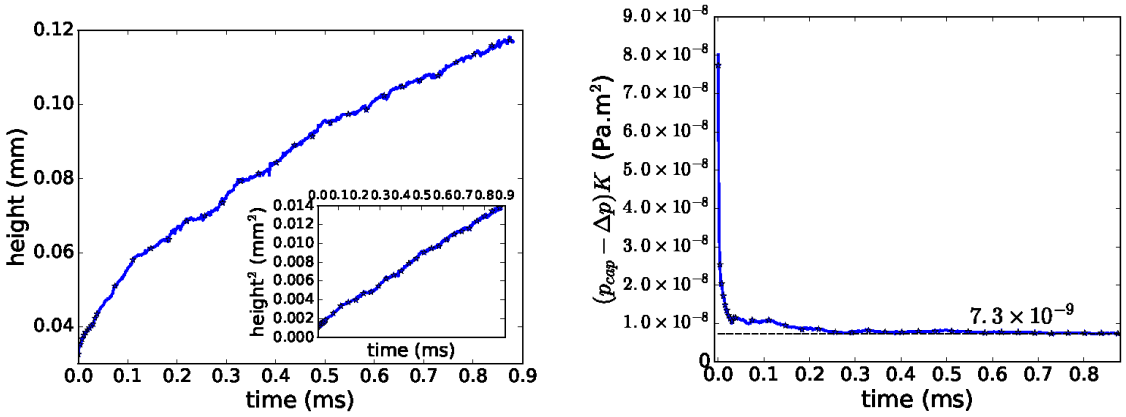

(a) $h(t)$ (b) $\eta_l h^2(t)/2t = (p_{cap} - \Delta p) \times K$

Figure 4: Capillary rise in a random structure : average position of the flow front over time (a) and corresponding values $p_{cap}K$ (b).

Figure 4a shows, as in the previous case, the average liquid height $h(t)$ and its square, $h^2(t)$, while the quantity $\eta_l h^2(t)/2t$, here equal to $(p_{cap} - \Delta p)K$, is reported in Figure 4b. Despite the random spacing of the fibres which impacts the liquid flow, it can be seen that h, again, behaves as the square root of time. Consequently, except just after the initial time $t = 0$ for which expression (16) is not valid, the quantity $(p_{cap} - \Delta p)K$ is constant, equal to 7.3×10^{-9} Pa.m^2, giving a capillary pressure $p_{cap} \approx 0.15$ bar or $p_{cap} \approx 5.2$ kPa, depending whether the permeability is provided by Method 1 or 2. Note that since Method 2 majorises the permeability, the corresponding capillary pressure is minorised. The capillary pressure values found here, lower than those obtained in the hexagonal structure, reflect the fact that capillary phenomena are less intense in this random structure. However, a more in-depth study is necessary, in

particular to know the influence that the pressure drop, imposed as boundary of condition, can have on these values, and thus be able to conclude on their relevance.

5 Conclusion

In this paper, a variational formulation of the Stokes system with capillarity was presented. Capillary effects are taken into account by considering a weak form of Laplace's law at the liquid - gas, liquid - solid and gas - solid interfaces, resulting in a weak imposition of the mechanical equilibrium at triple junctions. The mixed velocity - pressure system is discretised by using a stabilised finite element method. The computation of a saturated permeability is first carried out by numerical experiments, for a hexagonal structure - a good agreement with literature is found - and random 2D fibre structures. From the capillary rise simulations performed subsequently, a macroscopic quantity, the capillary pressure, can be calculated. However, while a spontaneous capillary flow was obtained in the case of the hexagonal structure, an additional driving force, *i.e.* a pressure drop, was required to force the liquid up into the random structure. Therefore, the continuation of this work will be, in the first place, the generation of random microstructures, with a controlled porosity as here, but satisfying additional constraints on the morphology of the arrangements, in particular the distance between two fibres, thus allowing spontaneous rises by capillarity.

REFERENCES

[1] K. Andriamananjara, N. Moulin, J. Bruchon, P.-J. Liotier, S. Drapier. *Numerical modeling of local capillary effects in porous media as a pressure discontinuity acting on the interface of a transient bi-fluid flow*. *Int. J. Mater. Form.* (2019) **12**:675–691.

[2] J. Bruchon, Y. Liu, N. Moulin. *Finite element setting for fluid flow simulations with natural enforcement of the triple junction equilibrium*. *Comput. Fluids* (2018) **171**:103–121.

[3] L. Chevalier, J. Bruchon, N. Moulin, P.-J. Liotier, S. Drapier. *Accounting for local capillary effects in two-phase flows with relaxed surface tension formulation in enriched finite elements*. *C.R. Mecanique* (2018) **346**(8):617–633.

[4] S. Badia, R. Codina. *Stokes, Maxwell and Darcy: A single finite element approximation for three model problems*. *Appl. Numer. Math.* (2012) **62**(4):246–263.

[5] R.F. Ausas, G.C. Buscaglia, S.R. Idelsohn. *A new enrichment space for the treatment of discontinuous pressures in multi-fluid flows*. *Int. J. Numer. Methods Fluids* (2012) **70**(7):829–850.

[6] F. Denner, B.G. van Wachem. *Numerical time-step restrictions as a result of capillary waves*. *J. Comput. Phys.* (2015) **285**:24–40.

[7] K. M. Pillai. *Governing equations for unsaturated flow through woven fiber mats. Part 1. Isothermal flows*. *Compos. Part A Appl. Sci. Manuf.* (2002) **33**(7) 1007–1019.

[8] L. Chevalier. *Accounting for capillary effects in level-set based Finite Elements modelling of impregnation in fibrous media*. *PhD thesis, École des Mines de Saint-Étienne* (2019).

[9] C. Mattrand, A. Béakou, K. Charlet. *Numerical modeling of the flax fiber morphology variability*, *Compos. Part A Appl. Sci. Manuf.* (2014) **63**:10–20.

[10] A. H. Coppola-Owen, R. Codina. *Improving Eulerian two-phase flow finite element approxima-*

tion with discontinuous gradient pressure shape functions, *Int. J. Numer. Methods Fluids* (2005) **12**:1287–1304.

[11] B. R. Gebart. *Permeability of unidirectional reinforcements for RTM*, *J. Compos. Mater.* (1992) **26**:1100–1133.

[12] P. C. Carman. *Fluid flow through granular beds*, *Trans. Inst. Chem. Eng.* (1937) **15**:150–166.